Earth Planet. Sci. Lett. 661 (2025) 119368

Contents lists available at ScienceDirect

Earth and Planetary Science Letters

journal homepage: www.elsevier.com/locate/epsl

The global imprint of shale weathering on molybdenum isotope ratios in river waters

Quentin Charbonnier [a,b,*], Edward T. Tipper [c], Robert G. Hilton [d], Corey Archer [a], Derek Vance [a]

[a] Department of Earth Sciences, ETH Zürich, Clausiusstrasse 25, 8092 Zürich
[b] Université de Paris, Institut de physique du globe de Paris, CNRS, 75005 Paris, France
[c] Department of Earth Sciences, University of Cambridge, Cambridge CB2 3EQ, United Kingdom
[d] Department of Earth Sciences, University of Oxford, Oxford OX1 3AN, United Kingdom

ARTICLE INFO

Editor: Dr H Bao

Keywords:
Weathering
Sulfide oxidation
River chemistry
Molybdenum isotopes

ABSTRACT

The molybdenum (Mo) isotope ratios (δ^{98}Mo) of marine sediments can preserve information on the redox state of the past ocean. However, a robust interpretation of marine δ^{98}Mo records requires an understanding of the main controls on the δ^{98}Mo values of riverine inputs. A growing consensus suggests that secondary mineral formation following rock weathering sets the δ^{98}Mo values of the dissolved riverine flux. However, variability in the Mo isotope composition of the weathering lithologies, such as sedimentary rocks, might exert an additional control. Here we assemble a dataset for large rivers spanning a wide range of sulfate abundance as a broad tracer of sulfide oxidation, making paired measurements of river water and solid loads.

The riverine dissolved and solid Mo isotopes span a range of +0.3 to +1.9 ‰ and -0.1 to +1.4 ‰, respectively. Our results indicate that both source and process control the isotope composition of dissolved riverine Mo. First, the elemental and isotope partitioning of Mo between river dissolved and solid loads is indicative of the impact of the formation of secondary weathering products. Second, the positive relationship between the dissolved and solid Mo isotope signatures implies the variable weathering of an additional heavy Mo isotope source above and beyond silicate. Consistent with this, silicate weathering alone cannot explain the riverine Mo abundances, calling for an additional Mo-rich source. Comparison between riverine dissolved Mo isotopes and potential sulfide oxidation tracers indicates an important control by sulfide weathering on river dissolved Mo isotope signatures. In this view, the pattern of variation of dissolved Mo isotopes across different weathering regimes may be interpreted in terms of the greater supply-limitation control of sulfide versus silicate weathering at the global scale. Overall, these findings indicate that changes in sulfide oxidation rates on the continents could modify the δ^{98}Mo of the global average riverine input to the oceans over geological timescales.

1. Introduction

The distribution of molybdenum and its isotopes (^{98}Mo/^{95}Mo, reported as δ^{98}Mo) in oceanic sedimentary archives has provided clear evidence of fluctuations in redox state in the ocean-atmosphere system over geological time (see review in Kendall et al., 2017). Molybdenum is mobile under oxic conditions (Mo VI; forming molybdate MoO_4^{2-} anion) and is slowly removed from the ocean by adsorption onto Mn-oxyhydroxides. In sulfidic environments, molybdate is quickly converted to particle-reactive thiomolybdate species that are subsequently removed via scavenging or (co)precipitation as solids (Kendall et al., 2017). Though changes in the redox state of Mo involve isotope fractionation, under the most reducing conditions Mo is quantitatively removed from solution, potentially yielding a record of oceanic Mo isotopes. Therefore, the quantification of the marine redox state extracted from sedimentary Mo isotope signatures requires a detailed understanding of the processes that control the Mo isotope composition of rivers, which provide the main input of Mo to the oceans (Archer and Vance, 2008). Consequently, the Mo isotope compositions of rivers have been subject to careful investigation in order to characterise this input (Archer and Vance, 2008; Pearce et al., 2010; Neubert et al., 2011; Rahaman et al., 2014; Wang et al., 2015; King and Pett-Ridge, 2018;

* Corresponding author.
E-mail address: quentin.charbonnier@univ-smb.fr (Q. Charbonnier).

https://doi.org/10.1016/j.epsl.2025.119368
Received 22 January 2025; Received in revised form 24 March 2025; Accepted 15 April 2025
Available online 28 April 2025

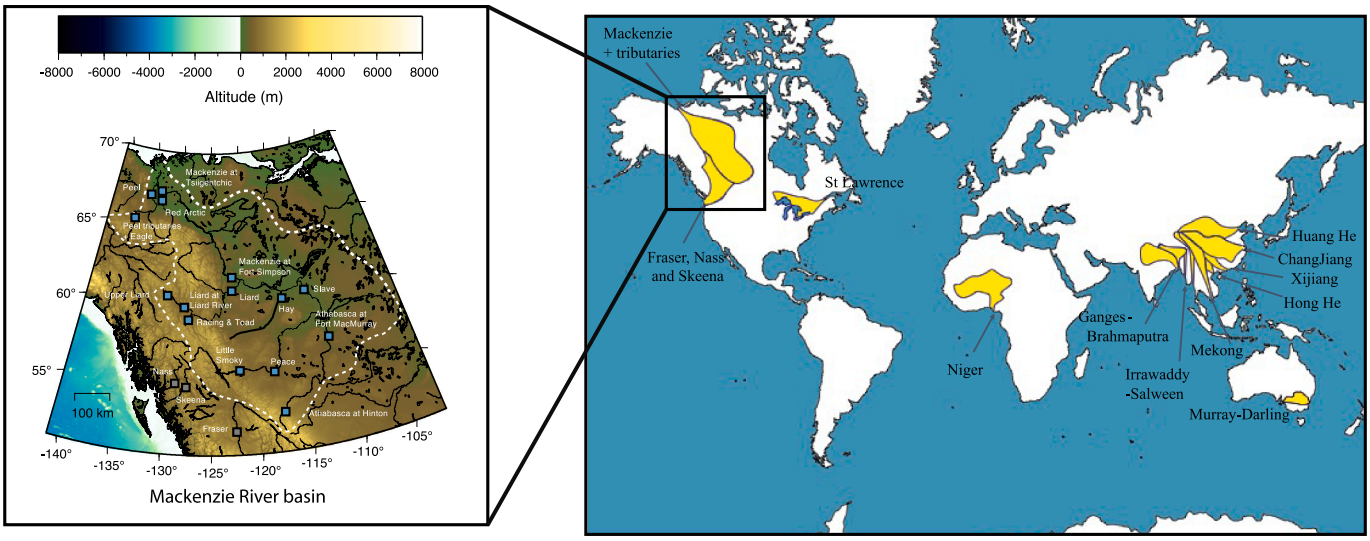

Fig. 1. Map of the basins sampled at their mouth for this study, as well as the details of the locations of sampling sites in the Mackenzie Basin. The "Peel tributaries" location merges the Eagle, the Ogilvie and the Blackstone rivers. Maps modified from Dellinger et al. (2014) and Gaillardet et al. (1999a).

Neely et al., 2018; Horan et al., 2020; Nägler et al., 2020; O'Sullivan et al., 2021; Revels et al., 2021). This work has demonstrated that the Mo isotope compositions of some of the world's largest rivers are significantly different from the continental crust (Archer and Vance, 2008). The extent of Mo uptake (and attendant isotope fractionation) by secondary phases following rock dissolution has been suggested to be responsible for this isotope difference (Archer and Vance, 2008).

A number of studies have since provided compelling evidence to support the important role of secondary mineral formation, and organic matter, in controlling δ^{98}Mo in streams and rivers (Wang et al., 2015; King et al., 2016; King and Pett-Ridge, 2018; Wang et al., 2018; Horan et al., 2020; Revels et al., 2021). However, there are limited data that allow us to quantify how weathering partitions Mo and its isotopes between the dissolved and particulate load of rivers, as opposed to partitioning between the total river load (dissolved and particulate) of rivers and soils (e.g., Wang et al., 2015). Furthermore, data compilations show that an additional control is likely the variability of the source rocks themselves (Horan et al., 2020). For example, since the Mo isotope signatures of the silicate rocks of the continental crust and those of sulfide minerals are distinct (Kendall et al., 2017; Willbold and Elliott, 2017; Fang et al., 2022), the relative amount of sulfide vs. silicate in the catchment bedrock should, in principle, contribute to the Mo isotopic signature of the dissolved load. The majority of riverine and soil δ^{98}Mo data are from catchments where organic carbon and sulfide rich-shales are insignificant, such as Iceland, Hawaii, the Amazonian plains and shields or soil profiles in China. In contrast, ~65 % of the continental surface is underlain by sedimentary rock (Hartmann and Moosdorf, 2012). Therefore, the potential lithological control on river dissolved Mo isotope signatures needs to be better addressed at a global scale (Pearce et al., 2010; Wang et al., 2015; King et al., 2016; King and Pett-Ridge, 2018; Wang et al., 2018; Revels et al., 2021). For instance, if sulfide mineral oxidation imparts an important control on δ^{98}Mo of rivers, secular changes in sulfide mineral oxidation could influence the Mo isotope mass balance of seawater. Sulfide oxidation rates have been shown to be highly sensitive to changes in geomorphic processes (Calmels et al., 2007; Bufe et al., 2021) and climatic variables (Walsh et al., 2024) and appear to have varied over timescales of 10 s to 100 s of million years (Torres et al., 2014; Rugenstein et al., 2019; Waldeck et al., 2022).

In this contribution, we investigate the influence of the oxidation of sedimentary rock-hosted sulfide on dissolved δ^{98}Mo values by comparing the dissolved and solid phase Mo isotope signatures of a set of large rivers, at their outlet, as well as some tributaries from the Mackenzie Basin. This compilation of rivers encompasses two orders of magnitude in dissolved sulfate concentrations, reflecting a wide range of lithological sources including sulfide-rich-shales, which are most important in the Mackenzie Basin (Huh et al., 2004; Calmels et al., 2007). The data derive from multiple continents: Northern America (St Lawrence, Skeena, Nass, Fraser and Mackenzie), South-east Asia (Ganges, Brahmaputra, Irrawaddy and one of its tributaries: Longjiang, Salween, Mekong and two of its tributaries: Nam Lik and Nam Hinboun, and Hong He), China (Changjiang, Xijiang and Huang He), Australia (Murray-Darling) and Africa (Niger).

We show that the variation in δ^{98}Mo in suspended sediment (~1 ‰) is mirrored by that in the dissolved load, but with a systematic offset of approximately 0.4 ‰ that is indicative of fractionation during weathering and the retention of light Mo isotopes in secondary minerals. In addition, we demonstrate that the variability in the dissolved Mo isotope composition cannot be explained solely by secondary weathering processes following silicate mineral dissolution. Furthermore, the combined river dissolved and solid loads reflect the variable contribution from sulfide oxidation to the riverine Mo elemental and isotope budget (Miller et al., 2011). A positive relationship is observed between δ^{98}Mo and previously reported tracers of sulfide oxidation such as SO_4 and osmium isotope ratios, suggesting that weathering of organic- and sulfide-rich shales is the additional source of Mo. Our study emphasises sulfide oxidation as an important input to the riverine Mo isotope budget, and that changing global rates of sulfide oxidation could modify seawater Mo isotope composition.

2. Material and methods

2.1. Sampling locations

Mo isotope ratios were measured in the dissolved, suspended and bed loads (where samples were available) in 17 of the world's largest river basins (Fig. 1). Large rivers integrate catchment geochemistry over continental scales and provide the best estimate of the composition of the land-to-sea fluxes at a scale relevant to global biogeochemical cycles (Gaillardet et al., 1999a).

In addition to the dataset for the large rivers, we report the Mo isotope composition of the dissolved and solid loads of Mackenzie Basin tributaries (Fig. 1). The Mackenzie Basin is the fourth largest Arctic river in terms of discharge (308 km^3/yr). The basin is underlain by two main geological provinces (excluding the Canadian Shield where weathering fluxes are minor). The Northern American Cordillera (Mackenzie and

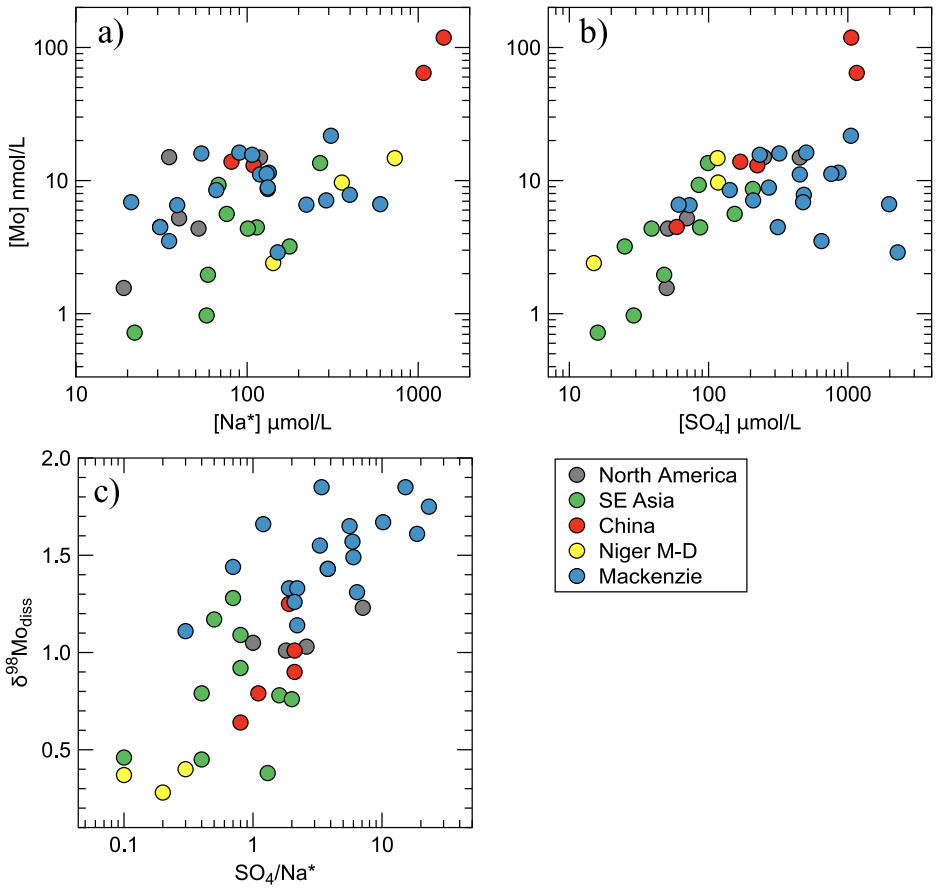

Fig. 2. Dissolved Mo concentrations vs. a) sodium (Na*) and b) sulfate (SO_4); c) dissolved Mo isotope composition ($\delta^{98}Mo_{diss}$) vs. SO_4/Na* ratio ("*" denotes Na concentrations after correction for sea-salt and evaporite inputs; Gaillardet et al. 1999b). North American rivers correspond to the Nass, Fraser, St Lawrence and Stikine; South East Asian rivers correspond to Nam Hinboun, Nam Lik, Mekong, Hong He, Longjiang, Irrawaddy, Salween, Ganges and Brahmaputra; Chinese rivers correspond to Changjiang at low and high water stages, Xijiang, and Huang He at low and high water stages; Niger and Murray Darling are merged together.

Rocky Mountains) has a range of elevation between 1000 and 2500 m. The main rock-types are Proterozoic to Mesozoic carbonates, dolomites, shales and black shales (Millot et al., 2003). The Interior Platform has an average elevation of 500 m, with bedrock comprising Cambrian to Cretaceous shales, black shales, limestones and evaporites (Millot et al., 2003). This study reports data for rivers draining the Rocky Mountains: Toad, Racing, Upper Liard, Athabasca (at Hinton), Ogilvie, Blackstone and Eagle. Two rivers drain only the Interior Platform: Hay and Little Smoky. Data are also reported for rivers (Red Arctic, Peel, Liard, Peace, Slave, Athabasca) that drain the Rocky Mountains as well as the Interior Platform, and that drain into the main Mackenzie channel. Data for the Mackenzie main channel are reported from two locations: Fort Simpson and Tsiigehtchic.

2.2. Sampling and elemental abundance determination

The samples analysed were collected during a number of different sampling campaigns (Gaillardet et al., 1999a; Lemarchand et al., 2002, 2003; Millot et al., 2003; Tipper et al., 2012; Dellinger et al., 2014; Horan et al., 2019, 2020; Tipper et al., 2020; Relph et al., 2021; Charbonnier et al., 2022a, 2022b, 2023, 2024). These previous papers detail sampling methods. Briefly, river waters were filtered within hours of sampling using Teflon lined or UPVC/polycarbonate filtration units with 0.2µ m filters (nylon or PES) into acid-washed polypropylene or HDPE containers. Water samples were acidified to pH ≈ 2 with ultra-pure HNO_3 and stored in a cold room. Major element concentrations were measured using ion chromatography (typical uncertainties are 1 to 3 %; Lemarchand et al., 2002; Gaillardet et al., 2003; Millot et al., 2003; Tipper et al., 2020; Relph et al., 2021). Mo concentration was determined using isotope dilution as part of this study.

The procedure for river solid sampling is described in Gaillardet et al. (1999a), Dellinger et al. (2014) and Tipper et al. (2020). For the Mackenzie Basin only, river solids were collected across a depth-profile from the river bottom to the near-surface (Dellinger et al., 2014). Such a sampling protocol provides access to the full spectrum of solid grain size, and by extension to the full mineralogy of river solid load (Bouchez et al., 2011). The river solids were recovered from the filter by scraping, or by rinsing the filter using filtered river water. River bed sediments were sampled from the bottom of the channel using a bucket. River solid samples were either dried at low temperatures (below 40°C) or freeze-dried. A mass of 50–100 mg of river solid was digested for at least 48 h using an HF-HNO_3 mix (3:1) in a Teflon beaker at 120°C. The solution was dried down and subsequently re-dissolved using *aqua regia,* to dissolve oxides and fluorides. The major and trace element concentrations of river sediments from the IPGP repository (such as the Mackenzie, Chinese, North American, Niger and G-B rivers) were determined at the SARM (Service d'analyse des Roches et des minéraux, INSU facility, Vandoeuvre les Nancy, France). Major elements were measured using ICP-OES, and trace elements using ICP-MS. The typical uncertainty is around 10 %. The major and trace element concentrations of other solid samples in this study (from Cambridge University), were determined using ICP-MS at the Institute of Geochemistry and Petrology of ETH Zürich.

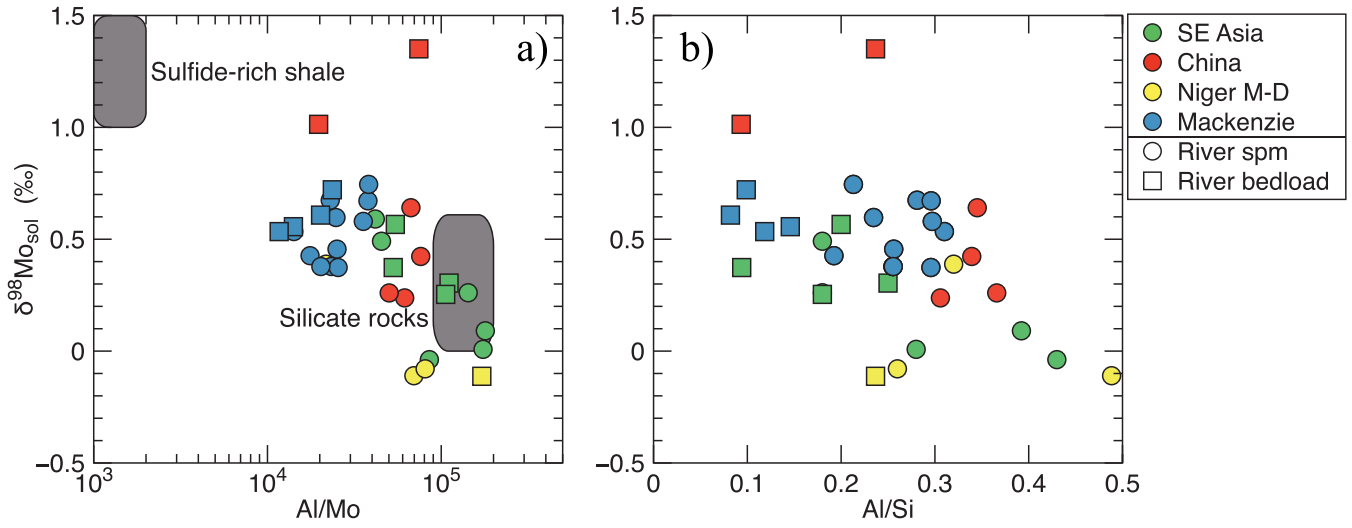

Fig. 3. Solid molybdenum isotope composition ($\delta^{98}Mo_{sol}$) vs. a) Al/Mo (ppm/ppm) ratio, and b) Al/Si ratio for suspended particulate matter (spm) and river bedload (rbl). The silicate rock endmember is inferred from Taylor and McLennan (1995), Willbold and Elliott (2017) and Fang et al. (2022) and sulfide-rich shale from Ross and Bustin (2009) and Kendall et al. (2017).

2.3. Mo isotope measurements

Molybdenum separation and isotope ratio measurements were performed at ETH Zürich, following Bura-Nakić et al. (2018). Briefly, an aliquot of sample (between 30 and 120 mL of river water and 10 mg of previously-digested river sediment) was spiked with an appropriate amount of a ^{100}Mo-^{97}Mo double spike (1:1 spike to sample ratio). The sample was evaporated to dryness and taken up in 1 M HCl. Molybdenum was separated using *Re*-resin (Bura-Nakić et al., 2018). Molybdenum isotope ratios were measured using a Thermo-Finnigan NeptunePlus (*MC-ICP-MS*) following Archer and Vance (2008) and reported relative to SRM NIST 3134 (Nägler et al., 2014):

$$\delta^{98}\mathrm{Mo} = \left[\frac{\left(^{98}\mathrm{Mo}/^{95}\mathrm{Mo}\right)_{smp}}{\left(^{98}\mathrm{Mo}/^{95}\mathrm{Mo}\right)_{std}} - 1\right] \times 1000 + 0.25 \quad (1)$$

The reproducibility and accuracy of the measurements were monitored via measurements of an in-house CPI standard with a range of standard/spike ratios (from 0.2 to 5) and the NIST standard. Data are reported here relative to NIST SRM3134 = + 0.25 ‰ (Nagler et al., 2014). The double spike was calibrated relative to a δ^{98}Mo = 0 ‰ for the CPI standard, and NIST SRM3134 gives +0.27±0.05 ‰ (average and 2 std dev, n = 155 over 7 years).

3. Results

Data for riverine dissolved and solid loads are reported in Supplementary Tables 1 and 2.

3.1. Major element and osmium concentrations, and radiogenic osmium isotope ratios

Variations in, and the lithological controls on, the major elements in the world's largest rivers, as well as those for the Mackenzie Basin, have been discussed previously (e.g., Gaillardet et al., 1999b; Millot et al., 2003). Briefly, sodium (Na) derives from silicate weathering, halite dissolution and sea salts (Gaillardet et al., 1999b). The contribution of sea salt is removed using the "critical" Cl value (a maximum of 20 µmol/L for large rivers; Gaillardet et al., 1999b) and the Na/Cl ratio of seawater. For Cl concentrations higher than 20 µmol/L, a contribution of halite/evaporite is required to explain the river dissolved Cl concentration. Thus, the Na from halite is corrected using the Cl concentration in excess of 20 µmol/L and the Na/Cl ratio of halite. Silicate Na (Na*), ranges from 20 µmol/L to 1415 µmol/L. Calcium (Ca), derived from carbonates, silicates and evaporites ranges from 112 µmol/L to 1561 µmol/L, and magnesium (Mg), originating from silicate and carbonate dissolution ranges from 63 to 1175 µmol/L. Sulfate (SO_4) is derived from aerosols, evaporites and sulfide weathering. Sulfate concentrations range from 15 µmol/L to 2281 µmol/L. Sulfate is correlated with Ca and Mg (not shown), reflecting the lithological control on SO_4, Ca and Mg (Millot et al., 2003; Calmels et al., 2007; Torres et al., 2014). Dissolved osmium abundances range from 26 (Skeena) to 202 *f*mol/L (Liard, Mackenzie Basin tributary), with the average for the Mackenzie Basin tributaries being significantly higher (113 *f*mol/L) than other large rivers (62 *f*mol/L; Levasseur et al., 1999; Sharma et al., 1999; Huh et al., 2004). Osmium radiogenic isotope ratios (^{187}Os/^{188}Os) span a range from 0.65 (Mekong) to 3.9 (Racing, Mackenzie Basin tributary), again with more radiogenic values for the Mackenzie Basin tributaries (2.0) than average large rivers (1.3).

3.2. Molybdenum and δ^{98}Mo in the riverine dissolved load

Dissolved Mo concentrations (Fig. 2) range from 0.7 nmol/L (Nam Hinboun, Mekong tributary sampled during monsoon) to 119 nmol/L (Huang He), with an average of 15 nmol/L, similar to the range reported for other large rivers (around a few nmol/L except for the Huang He; Archer and Vance, 2008; Rahaman et al., 2014; Wang et al., 2015; Horan et al., 2020; O'Sullivan et al., 2021; Revels et al., 2021), and small rivers that have been sampled across a broad range of climate conditions (Pearce et al., 2010; Neubert et al., 2011; Voegelin et al., 2012; King and Pett-Ridge, 2018; Horan et al., 2020). The dissolved Mo abundance shows a weak positive relationship with sodium derived from silicate in log-log space (Fig. 2a), as previously shown for the Amazon Basin (Revels et al., 2021). Similar to previous data from large rivers, the dissolved Mo abundances show a broad positive relationship with sulfate in log-log space (Fig. 2b; Miller et al., 2011).

The δ^{98}Mo of the dissolved load (Fig. 2c) ranges from 0.3 ‰ (Darling) to 1.9 ‰ (Ogilvie) with a non-weighted average value of 0.8 ‰, within uncertainty of the value for the global riverine flux estimated in Revels et al. (2021). The values reported for the Huang He, Xijiang and Changjiang are consistent with those reported in Wang et al. (2015). This range of values is higher than that for the average continental crust (+0.0–0.6 ‰, estimated using igneous rocks and terrigenous sediments and referred to as silicates in the figures; Willbold and Elliott, 2017;

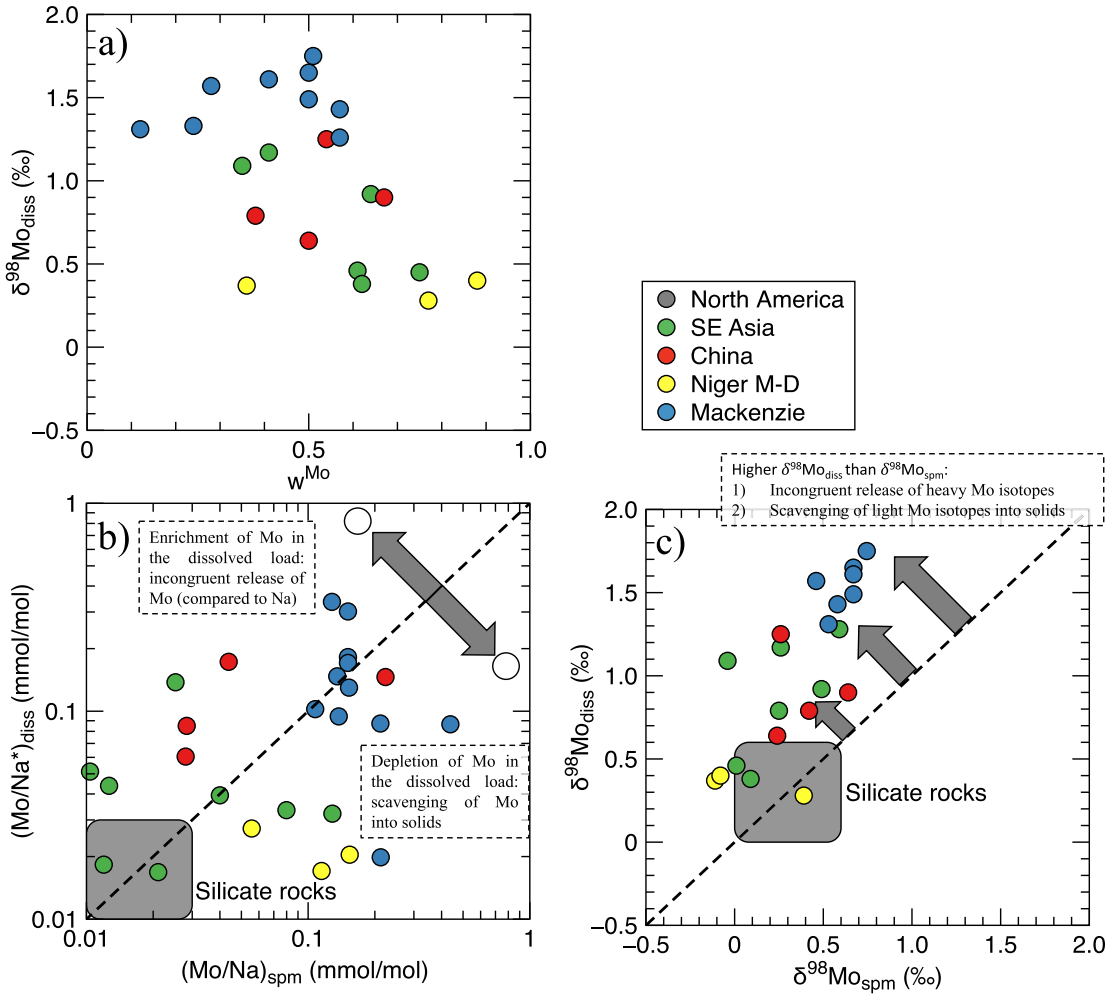

Fig. 4. a) Fraction of Mo exported as dissolved species (w^{Mo}; eq. (2)) vs. $\delta^{98}Mo_{diss}$, b) comparison between Mo/Na in river dissolved load and spm, c) $\delta^{98}Mo$ of dissolved load and spm. Normalisation to Na allows comparison of the riverine dissolved and solid phase Mo fluxes. The silicate rock endmember is inferred from Taylor and McLennan (1995), Willbold and Elliott (2017) and Fang et al. (2022).

Fang et al. 2022), consistent with the data compilation for large rivers (Archer and Vance, 2008; Kendall et al., 2017). The Mackenzie Basin tributaries exhibit the highest $\delta^{98}Mo$ values (around 1.5 ‰, on average). The rivers from North America, China and South-East Asia (except G-B and Irrawaddy) show intermediate values (between 0.8 and 1.2 ‰), while the Niger, Murray-Darling, G-B and Irrawaddy show the lowest values (around 0.4 ‰; closest to the $\delta^{98}Mo$ value of the continental crust). A broad positive trend is observed between dissolved load $\delta^{98}Mo$ and SO_4/Na^* ratios (Fig. 2c).

3.3. Molybdenum and its isotopes in the riverine particulate load

The Mo concentration in river suspended particulate matter (spm) and bed load (rbl) of the rivers analysed ranges from 0.2 to 5.6 mg/kg, which exceeds the range measured in silicate rocks (1.0–1.5 mg/kg; Taylor and McLennan, 1995; Rudnick and Gao, 2013). However, the abundance of chemical species in river solids is strongly influenced by the quartz content (Bouchez et al., 2011), referred to as quartz dilution. To take this quartz dilution into account, the Mo concentration in the solid is normalised to aluminium (Al), an immobile element not hosted in quartz. The Mo/Al of the two main models of silicate rocks that make up the modern continental crust, namely siliciclastic sedimentary and igneous rocks (see Taylor and McLennan, 1995; Rudnick and Gao, 2013), are merged together and plotted for comparison (referred to as silicate rocks in the text and figures). The Mo/Al ratios of river solids are always greater than or equal to those of silicate rocks (Fig. 3a).

The $\delta^{98}Mo$ value of river solids ranges from −0.1 to 1.4 ‰ (Fig. 3a), both lower and higher than the average of silicate continental crustal rocks (+0.0–0.6 ‰; Willbold and Elliott, 2017; Fang et al. 2022). Overall, the Mackenzie Basin and two Chinese rivers show the highest $\delta^{98}Mo$, while some of the South-East Asian and the other Chinese rivers show slightly lower $\delta^{98}Mo$ values. Finally, the Niger, Murray, Darling and some of the South-East Asian rivers show $\delta^{98}Mo$ values close to or lower than silicate rocks. There is a broad negative trend between $\delta^{98}Mo$ and Al/Mo (Fig. 3a), and a broad negative relationship between $\delta^{98}Mo$ and Al/Si, a tracer of sediment grain size, with Al-rich samples corresponding to fine clays and Si-rich samples to quartz and coarse, more quartz-rich, sediments (Bouchez et al., 2011; Fig. 3b).

3.4. Mo elemental and isotope partitioning between the dissolved and solid loads

The relative fraction of Mo transported as a dissolved species can be estimated using:

$$w^{Mo} = \frac{[Mo]_{diss}}{[Mo]_{diss} + [Mo]_{spm} \times [spm]} \quad (2)$$

where $[Mo]_{diss}$ is the dissolved Mo concentration (in µg/L), $[Mo]_{spm}$ the Mo concentration in river suspended sediments (in mg/kg), and $[spm]$

the long-term suspended particulate matter concentration in g/L. The fraction of Mo transported as a dissolved species ranges from 12 (Arctic Red) to 89 % (Murray), with an average value of 50 % (Fig. 4a). This result indicates the importance of dissolved Mo to the total Mo load in rivers, consistent with findings from Revels et al. (2021). A broad negative relationship emerges between the fraction of Mo transported as dissolved species (w^{Mo}) and dissolved Mo isotopes (Fig. 4a), for which high w^{Mo} coupled with low $\delta^{98}Mo_{diss}$ are consistent with the congruent weathering of silicate rocks.

Given the wide range of climate regimes (runoff and evaporation) covered by the rivers in our dataset, dilution is likely to be a key control on all elemental abundances. To eliminate this effect, the data are presented as elemental ratios, which are independent of dilution (Fig. 4b). Mo/Na* ratios in the dissolved load, $(Mo/Na^*)_{diss}$, show a range from 0.01 (Eagle) to 0.43 (St Lawrence) mmol/mol. Here the Mo/Na ratios of the two main models of silicate rocks making up the modern continental crust, siliciclastic sedimentary and igneous rocks, are reported together (see Taylor and McLennan, 1995; Rudnick and Gao, 2013). Most rivers exhibit higher $(Mo/Na^*)_{diss}$ and $(Mo/Na^*)_{spm}$ (suspended particulate load) ratios than silicate rocks (0.01–0.03 mmol/mol; Taylor and McLennan, 1995; Rudnick and Gao, 2013). There is no clear pattern between $(Mo/Na^*)_{diss}$ and $(Mo/Na)_{spm}$ (Fig. 4b).

There is a positive relationship between $\delta^{98}Mo_{diss}$ and $\delta^{98}Mo_{spm}$ (Fig. 4c). The slope of the linear correlation is greater than 1, and it is displaced from a 1:1 line towards higher $\delta^{98}Mo_{diss}$, indicating that the dissolved load is systematically enriched in ^{98}Mo relative to suspended particulate matter.

4. Discussion

Most of the river dissolved and solid loads show elevated $\delta^{98}Mo$ relative to average silicate rocks. The fact that the Mo elemental and isotope ratios are distinct between the river dissolved and solid loads suggests fractionating processes in the weathering environment (Archer and Vance, 2008; Wang et al., 2015; Horan et al., 2020; Revels et al., 2021). However, no single relationship emerges between dissolved Mo/Na* and $\delta^{98}Mo$ (see Supplementary Fig; Revels et al., 2021). Moreover, the higher $\delta^{98}Mo$ values are accompanied by elemental enrichment of Mo in both river dissolved and solid loads. Such a systematic enrichment in riverine Mo, coupled to heavy Mo isotopes also, therefore, hints at an additional Mo source beyond silicate, with a different Mo isotope signature.

The broad positive relationship between dissolved Mo isotopes and SO_4/Na^* ratio suggests that sulfate sources, such as organic-rich, sulfide-rich shale or gypsum could provide this heavy isotope Mo source (Fig. 2c). Overall, the results suggest a role for both weathering process and source in setting riverine fluxes of Mo and Mo isotopes, the latter especially clear for the Mackenzie Basin, as has already been highlighted (Horan et al., 2020). Herein, we seek to address the relative importance of source and process by investigating first the variation of Mo isotopes in river solid loads, and second the complementarity between river dissolved and solid loads. After demonstrating a lithological control on riverine Mo isotope signatures, we show that sulfide oxidation contributes to the higher dissolved $\delta^{98}Mo$ for the largest rivers in the world and could impact the global Mo isotope mass balance of seawater.

4.1. Lithological versus weathering fractionation controls on riverine $\delta^{98}Mo$

Previous studies (e.g., Archer and Vance, 2008; Neubert et al., 2011; King et al., 2018; Revels et al., 2021) have generally used only dissolved load Mo and Mo isotope data to assess the controls on riverine Mo. Here, we also examine river bedloads and suspended particulate matter to provide further insight into the source control, via the elemental and isotope compositions of the weathered bedrock (e.g., Bouchez et al., 2011; Dellinger et al., 2014; Fig. 3).

The pattern of variation observed between Al/Mo and $\delta^{98}Mo$ (Fig. 3a) could reflect binary mixing, between a silicate end-member with high Al/Mo and an inferred $\delta^{98}Mo$ of 0.0–0.4 ‰ consistent with the literature (see estimate in Willbold and Elliott, 2017 and Fang et al., 2022), and an end-member with lower Al/Mo ratio representing contributions from a Mo-rich source with a heavy isotope signature. As for the Mo/Na ratio of the silicate endmember, the modern silicate crust is made up of recycled sedimentary silicate and igneous rocks (e.g., Gaillardet et al., 1999a) for which 1) individual $\delta^{98}Mo$ values for rock samples vary widely and 2) could be distinct between igneous and sedimentary rocks due to past weathering cycles (see the variability for individual samples in e.g., Kendall et al., 2017; Willbold and Elliott, 2017; Ye et al., 2021 and Fang et al., 2022). The relatively restricted range of extrapolated silicate $\delta^{98}Mo$ using river solid load is attributable to the fact that large rivers represent the weighted average of source rock compositions, thereby mitigating the variability of individual igneous and sedimentary silicate samples reported in the literature. Regarding the additional Mo endmember, it seems more dominant across the Mackenzie Basin tributaries (Fig. 3a). The Mackenzie Basin is known to be highly influenced by weathering of carbonate and sulfide- or organic-rich shale (Millot et al., 2003; Huh et al., 2004; Horan et al., 2019; Charbonnier et al., 2022a, 2023). Given the low concentration of Mo in carbonate (Clarkson et al., 2020), and the relatively low carbonate content of river sediment (compared to silicate-derived phases), it is unlikely that carbonate could represent this additional source. Hence, the second endmember is more likely to be sulfide- or organic-rich shale (Neubert et al., 2011). The range of $\delta^{98}Mo$ values for sulfide-rich shale is narrow in comparison to the entire range of individual rock samples (see compilation in Ye et al., 2021). Again, the extrapolated endmember is likely to reflect the weighted average of the sulfide-rich shale endmember at the global scale. We return to this point later in the discussion.

A negative relationship between particulate $\delta^{98}Mo$ and Al/Si ratio also sheds light on the composition of average rocks undergoing weathering in the catchments. Samples with lower Al/Si ratios, mostly found in the bedload (Fig. 3), correspond to coarse and less weathered river solids. Lower $\delta^{98}Mo$ are mainly found for the highest Al/Si ratios, thought to represent the most secondary weathering product-rich samples (Bouchez et al., 2011). Though the dataset in Fig. 3b is small, there may be greater scatter in the Mo isotope composition of the low Al/Si particulate load samples (bedload, most representative of the bedrock source), also suggesting variable contributions from more than one bedrock source.

These conclusions from the suspended load data are re-enforced by a further comparison between Mo and Mo isotopes of the suspended and dissolved loads (Fig. 4b,c). The positive relationship between $\delta^{98}Mo_{diss}$ and $\delta^{98}Mo_{spm}$ extends away from the low $\delta^{98}Mo$ values expected of silicate minerals. The co-evolution of both dissolved and solid phases supports a role of a sulfide-rich shale input whose contribution differs across the sample set. Further, the range of dissolved Mo abundances in most rivers (relative to that of Na, a soluble element deriving from silicate and not influenced by secondary mineral formation) also indicates that silicate weathering on its own cannot explain the dissolved Mo abundance in rivers (Fig. 4b).

Besides the variable contribution from an additional heavy Mo isotope source, there is also a need for an additional control from Mo and Mo isotope partitioning into secondary minerals formed in the weathering environment. The $\delta^{98}Mo_{diss}$ values are systematically higher than the corresponding $\delta^{98}Mo_{spm}$ (Fig. 4c), indicating isotope fractionation due to scavenging of light Mo isotopes into secondary weathering products (e.g., Archer and Vance, 2008; Horan et al., 2020; Revels et al., 2021). The river dissolved $(Mo/Na)^*$ ratio, though higher than that of silicate, is often lower than the corresponding riverine particulate matter (Fig. 4b). This confirms that a significant fraction of Mo (either released by silicate or the additional source) is removed by secondary phase formation (e.g. Archer and Vance, 2008; Wang et al., 2015; Horan

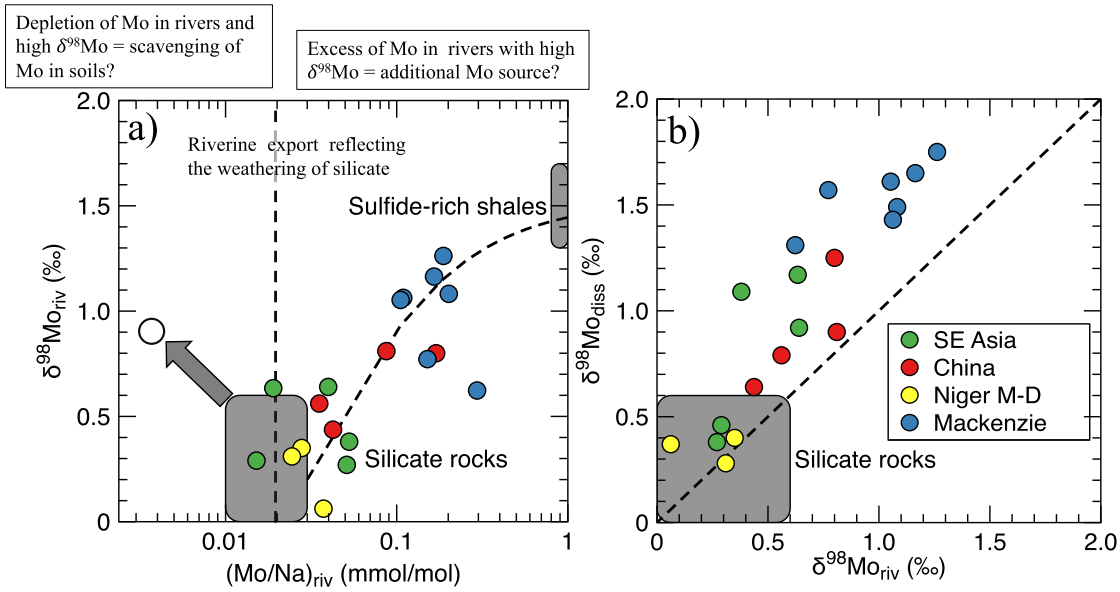

Fig. 5. a) Mo isotope composition of total riverine export ($\delta^{98}Mo_{riv}$) vs. the riverine export of Mo relative to sodium ($(Mo/Na)_{riv}$) and b) the Mo isotope composition of the river dissolved loads ($\delta^{98}Mo_{diss}$) vs. the Mo isotope composition of the total riverine export ($\delta^{98}Mo_{riv}$). The Mo/Na ratio and Mo isotope composition of silicate are inferred from Taylor and McLennan (1995), Rudnick and Gao (2013), Willbold and Elliott (2017) and Fang et al. (2022). The range of Mo/Na and Mo isotope composition of sulfide-rich shale is inferred from Ross and Bustin (2009) and Kendall et al. (2017). The detail of calculations is given in Appendix.

et al., 2020; Revels et al., 2021).

4.2. Constraints from overall riverine mass budgets

Some of the conclusions in the previous section are potentially compromised by the preferential retention of light Mo isotopes in soils or regolith (Archer and Vance, 2008; Pearce et al., 2010; Wang et al., 2015; King et al., 2018). This would act to introduce a third reservoir for Mo released during weathering, in addition to the suspended and dissolved loads of rivers and complicating the mass balance. In this section, we explore the combined dissolved and particulate loads, to assess the degree to which the overall riverine export flux is consistent with the dual controls introduced in previous sections: source versus weathering process. In this analysis (see Appendix for details), the elemental river mass budget is considered in terms of the total Mo/Na ratio exported by rivers $(Mo/Na)_{riv}$. The Mo isotope composition of the total river flux is referred to as $\delta^{98}Mo_{riv}$.

There is a broad positive relationship between $(Mo/Na)_{riv}$ and $\delta^{98}Mo_{riv}$, from values close to the Mo elemental and isotope composition of silicate rocks towards higher Mo riverine export combined with heavier Mo isotope signatures (Fig. 5a). The coupled increase in the riverine export of Mo and in heavy Mo isotopes - over and above that expected from silicates - lie close to a theoretical binary mixing relationship between 1) silicate rocks and 2) most likely a sulfide-rich shale, having an extrapolated Mo isotope composition of around 1.5 ‰.

Again, however, we also note that, though $\delta^{98}Mo_{riv}$ is positively correlated with $\delta^{98}Mo_{diss}$, $\delta^{98}Mo_{diss}$ is systematically higher by around $+0.4 \pm 0.4$ ‰ compared to $\delta^{98}Mo_{riv}$ (Fig. 5b). These findings again

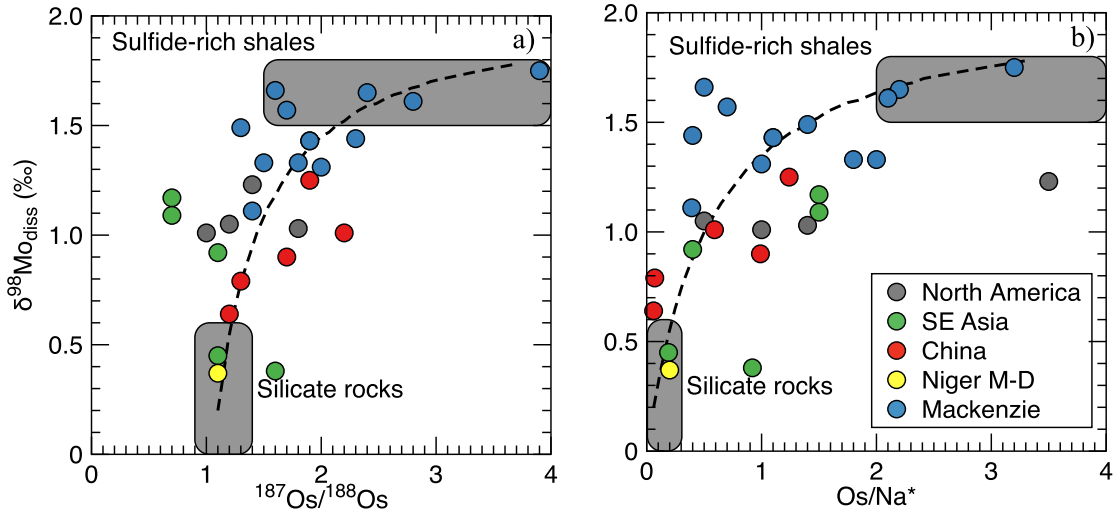

Fig. 6. Dissolved Mo isotope compositions ($\delta^{98}Mo_{diss}$) vs. a) radiogenic osmium isotope ratios ($^{187}Os/^{188}Os$) and b) Os/Na* ratio. Osmium data are from Levasseur et al. (1999), Sharma et al. (1999) and Huh et al. (2004). The dashed curves are predicted mixing relationships using end-member $^{187}Os/^{188}Os$ and Os/Na* for silicate and organic-rich shale as estimated in Levasseur et al. (1999) and Huh et al. (2004). Note that all data on these plots come from the same samples except for the Southeast Asian rivers (green) and a few Mackenzie tributaries.

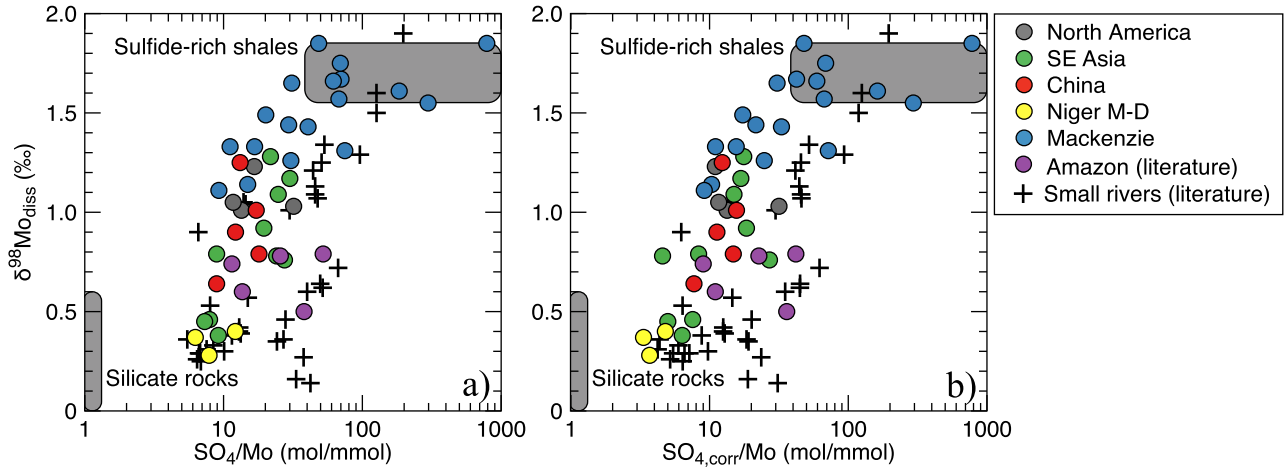

Fig. 7. Dissolved Mo isotope composition ($\delta^{98}Mo_{diss}$) vs. a) raw SO_4/Mo ratios and b) SO_4/Mo corrected for gypsum and rain inputs (when possible - see text). Literature data come from Neubert et al. (2011), Horan et al. (2020) and Revels et al. (2021). The silicate endmember is inferred from Taylor and McLennan (1995), Rudnick and Gao (2013), Willbold and Elliott (2017) and Fang et al. (2022). The sulfide endmember is from Miller et al. (2011) and Kendall et al. (2017).

imply that $\delta^{98}Mo_{diss}$ reflects both source and incorporation of light Mo into secondary weathering products or adsorption onto organic matter. As with other aspects of the dataset, the Mackenzie samples in particular show the highest $\delta^{98}Mo_{riv}$ (indicative of a dominant contribution from sulfide-rich shale). In contrast, secondary weathering processes are the dominant controlling factor in basins for which Mo is sourced by silicate weathering only (as represented by the river having a $\delta^{98}Mo_{riv}$ close to silicate values).

4.3. River dissolved Mo isotope signatures as a tracer of sulfide-rich shale weathering?

The previous section suggests that variability in riverine dissolved Mo isotopes can be partly attributed to the variable contribution from silicate and sulfide-rich shale. The corollary is that dissolved Mo isotopes could potentially be used to trace silicate weathering vs. sulfide oxidation, which have contrasting roles in the geological carbon cycle (e.g., Torres et al., 2014).

In this section, we use data from additional tracers to investigate this hypothesis further.

The radiogenic isotope ratio of osmium ($^{187}Os/^{188}Os$) is known to exhibit distinct signatures in silicate crust ($^{187}Os/^{188}Os \approx 1.0–1.4$; Peucker-Ehrenbrink and Jahn, 2001) versus organic-rich sedimentary rocks ($^{187}Os/^{188}Os > 1.5$; Huh et al., 2004). The hyperbolic trends between $\delta^{98}Mo_{diss}$ vs. $^{187}Os/^{188}Os$ and $\delta^{98}Mo$ vs. Os/Na^* (Fig. 6) are consistent with binary mixing between Mo and Os released from silicates ($^{187}Os/^{188}Os \approx 1$ and $Os/Na^* \approx 0.4$ *f*mol/μmol) and from sulfide- or organic-rich shale ($^{187}Os/^{188}Os > 1.5$ and $Os/Na^* > 1$ *f*mol/μmol). We note that given the wide range of $^{187}Os/^{188}Os$ values for the silicate and black shale endmembers, the modelled trends between $\delta^{98}Mo_{diss}$ vs. $^{187}Os/^{188}Os$ only provide qualitative information. Conversely, the mixing trend between Os/Na^* and $\delta^{98}Mo_{diss}$ corresponds to a mixing model using the lowest and highest Os/Na^* to define silicate and sulfide-rich shale. Besides potential variability in the end-members, the scatter about the theoretical mixing could also reflect the influence of secondary weathering processes.

Sulfate measurements provide additional support for the suggestion that riverine $\delta^{98}Mo$ values partly reflect oxidative weathering of shales. A relationship between dissolved SO_4/Na^* and $\delta^{98}Mo_{diss}$ (Fig. 2c) has previously been linked to sulfide oxidation (Miller et al., 2011). However, sulfate in rivers derives from a number of sources: sulfide oxidation, gypsum dissolution and atmospheric inputs (e.g., Spence and Telmer, 2005). Here, we use the contribution of SO_4 deriving from sulfide oxidation from previous studies (estimated using sulfur-oxygen or carbon isotope systems; Galy and France-Lanord, 1999; Spence and Telmer, 2005; Calmels et al., 2007; Relph et al., 2021), where available, and then examine sulfide oxidation derived SO_4 for large and small rivers (data from Horan et al., 2020; Revels et al., 2021; Supplementary Table 3; Fig. 7). For rivers where such data are not available, a first-order correction is performed to dissolved SO_4 using dissolved Cl deriving from sea salt (using the critical Cl value) and evaporites and the SO_4/Cl ratio of precipitation from Stallard and Edmond (1981) and Miller et al. (2011) (≈0.33), and the sea water ratio for gypsum.

Riverine dissolved $\delta^{98}Mo$ shows a broad positive relationship with both the uncorrected and corrected SO_4/Mo (Fig. 7a,b). Extrapolation of endmembers using the SO_4/Mo ratios (Miller et al., 2011) gives, again, a silicate and sulfide-rich shale $\delta^{98}Mo$ of 0.0–0.4 ‰ and 1.6–1.8 ‰, respectively, that is consistent with the endmembers inferred from other mixing relationships (see above). Similar to the osmium vs. $\delta^{98}Mo$ cross-plot, secondary weathering processes likely cause the scatter in the relationship. The range in Mo isotope composition for the inferred sulfide endmember is relatively narrow compared to that of the literature (Ye et al., 2021), the latter ranging from −2.0 ‰ to +2.3 ‰ and thus overlapping the range for silicate. It appears that large river systems integrate and average the diversity of elemental and isotope signature of lithological endmembers (Négrel et al., 1993).

Altogether, the Mo and Mo isotope river mass budget results, as well as the comparison between riverine dissolved Mo isotopes and silicate vs. sulphide-rich shale tracers, support the hypothesis that variable contributions of silicate and sulfide-rich shale impose an important control on the dissolved Mo isotope signatures in rivers from this study. Therefore, dissolved Mo isotopes may help to assess the contribution of silicate weathering vs. sulfide oxidation to the weathering budget through Earth's history. In the next section we address the role that weathering regimes might play in the riverine dissolved Mo isotope signature and, by extension, on the silicate vs. sulfide contribution to the world's largest rivers.

4.4. Modern and past weathering regime changes as a controlling factor of Mo isotope fluxes

The extent to which secondary weathering processes fractionate the stable isotope ratios of metals is thought to be controlled by the weathering regime (e.g., Li or U, Dellinger et al., 2015b; Charbonnier et al., 2023). In this view, a previous study has also proposed a similar control on riverine dissolved $\delta^{98}Mo$ (Revels et al., 2021). However, sulfide oxidation is itself thought to be limited by the supply of fresh

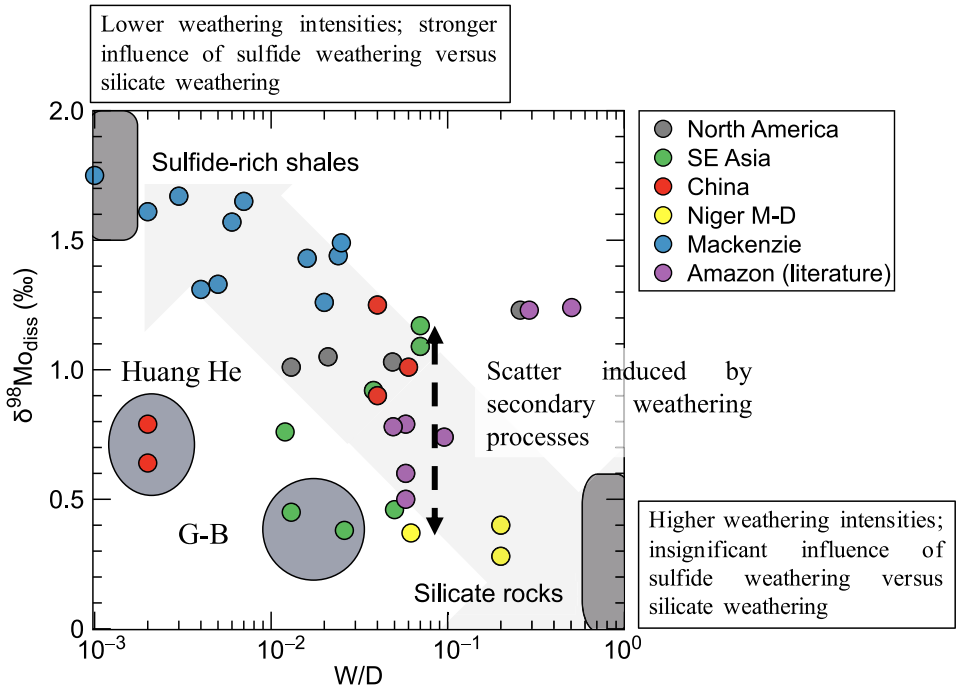

Fig. 8. Weathering intensity (W/D) vs. dissolved Mo isotope compositions ($\delta^{98}Mo_{diss}$). Weathering intensity corresponds to the depletion of silicate-derived cations from the solid (Bouchez et al., 2014). W/D data are from Gaillardet et al. (1999b), Dellinger et al. (2015b) and Dellinger et al. (2017). Amazon data come from Revels et al. (2021).

materials (tectonic control), whereas silicate weathering is limited by the dual control of both climate and tectonic factors (West et al., 2005; Calmels et al., 2007). Thus, if dissolved Mo isotopes are also partly controlled by silicate vs. sulfide weathering, a link between weathering regime and dissolved Mo isotopes might, alternatively, be driven by this control on sulfide vs. silicate weathering by weathering regime. To investigate a potential causal relationship between Mo isotopes and weathering regimes, dissolved Mo isotope compositions are compared to the weathering intensity (W/D ratios; Bouchez et al., 2014).

The weathering intensity (W/D) corresponds to the silicate weathering flux (W; estimated with the flux of silicate-derived cations in the river dissolved load; Gaillardet et al., 1999b) relative to the total denudation flux (i.e. the sum of dissolved and solid materials exported by rivers). Low W/D ratios correspond to low silicate weathering flux relative to the supply of fresh material to the weathering reactor, because of the kinetic limitation of silicate weathering (West et al., 2005). In contrast, high W/D ratios correspond to near-complete solubilisation of base cations from silicate rocks, so that the weathering reactions are limited by the supply of fresh materials.

A broad negative relationship emerges between the $\delta^{98}Mo_{diss}$ and W/D ratios (Fig. 8). In principle, this relationship could correspond to the variable extent of Mo scavenging phase formation (leading to higher $\delta^{98}Mo$; see Revels et al., 2021) across different weathering regimes. Nonetheless, theoretical models, supported by evidence from lithium isotope systematics (a tracer of secondary weathering product extent; Dellinger et al., 2015b), suggest that kinetic limitations lead to minimal secondary weathering at low W/D (e.g., Bouchez et al., 2013), while intermediate and higher W/D (with some exceptions for very high W/D) favour the formation of secondary weathering products. Therefore, the trend between $\delta^{98}Mo_{diss}$ and W/D is not fully compatible with a control exclusively related to the scavenging of light Mo isotopes by secondary weathering products.

Instead, higher $\delta^{98}Mo_{diss}$ found for low W/D, where the total export of material greatly outpaces the silicate weathering fluxes, may correspond to stronger contributions of sulfide oxidation relative to silicate weathering to the riverine Mo budget. In contrast, the more complete conversion of rocks into soluble cations and secondary weathering products through chemical weathering (elevated W/D ratios) yields Mo isotope signatures closer to that of silicate rocks. This is consistent with the insignificant contribution of sulfide oxidation to the weathering budget of Mo at high W/D ratios. Again, the scatter on Fig. 8, and the shift compared to the silicate and sulfide endmembers, can be attributed to secondary phases produced during weathering (see Fig. 5b). Some rivers clearly lie off the main trend on Fig. 8, such as the Huang He. However, the physical and chemical weathering rates in the Huang He are not at steady-state (Gaillardet et al., 1999b; Charbonnier et al., 2022b), most likely because of a recent increase in the erosion rates. This translates into W/D much lower than expected. Furthermore, the Ganges and Brahmaputra also shows lighter dissolved $\delta^{98}Mo$ compared to the trend. The exact reason for this is unclear, as these rivers are known to be influenced by sulfide weathering (Galy and France-Lanord, 1999). A potential explanation could be the weathering of metasediments (e.g., Dellinger et al., 2014) with a Mo isotope composition that may be shifted from unmetamorphosed black shales. In addition, some of the Amazonian Shield tributaries lie off the trend toward heavier Mo isotope values. Shields are virtually free of sulfide-rich shale, so that these rivers may be exclusively controlled by secondary weathering products with minimal source control.

Therefore, the pattern observed between W/D and the relative contribution of sulfide oxidation vs silicate weathering – broadly traced here using dissolved Mo isotope signatures – is consistent with previous studies underscoring the supply limitation of sulfide oxidation (ie. promoted by increases in the denudation rates; Calmels et al., 2007; Torres et al., 2014), while the increase in silicate weathering flux relative to total denudation (higher W/D) tends to counteract the influence of sulfide oxidation. Though the link between sulfide oxidation and weathering regime has been suggested in restricted areas only (e.g., Torres et al., 2014, 2016, 2017), evidence from our analysis might support this link in some other large rivers, suggesting that it ought to be investigated further in other rivers featuring low W/D.

To illustrate how these variabilities in weathering intensity might have theoretically imprinted the sedimentary $\delta^{98}Mo$, we consider a

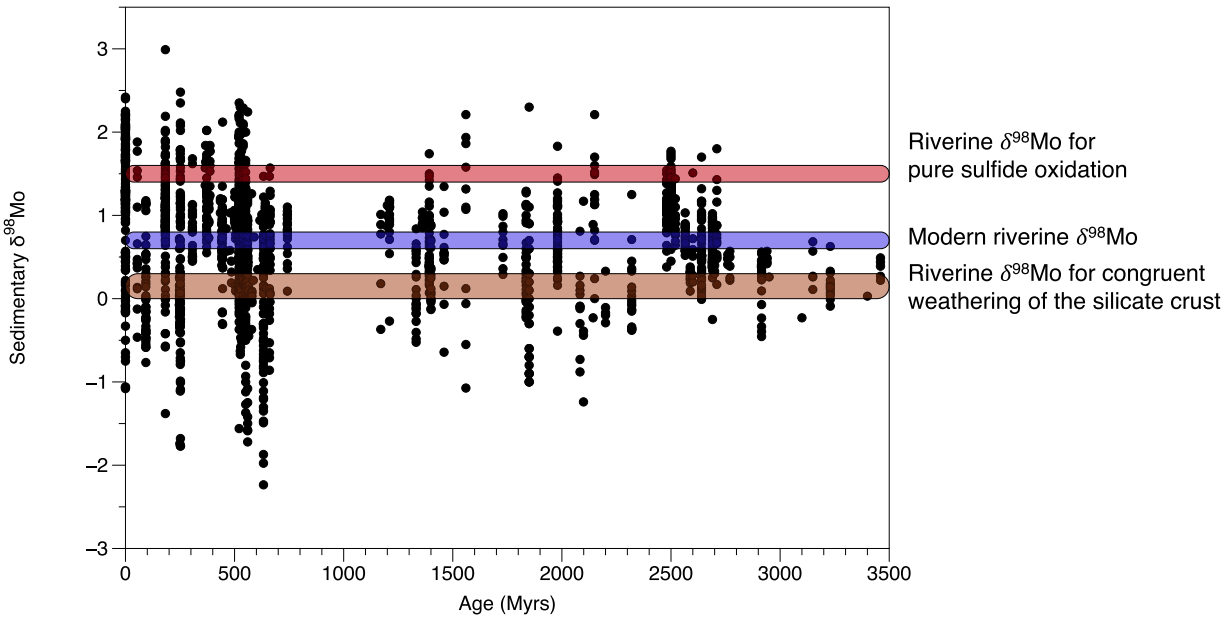

Fig. 9. Global compilation of sedimentary δ^{98}Mo reported in Ye et al. (2021). The coloured bands represent 1) the riverine δ^{98}Mo input to the ocean for a riverine flux wholly derived from sulfide oxidation (red) assuming that the δ^{98}Mo value for sulfide oxidation is similar to the modern one, 2) the modern riverine δ^{98}Mo (blue) from Revels et al. (2021) and 3) riverine δ^{98}Mo in the case of congruent weathering of silicate only (brown), yielding values similar to the continental crust.

recent global compilation of δ^{98}Mo in sediments (Fig. 9) (Ye et al., 2021). The congruent weathering of silicates at high weathering intensity should result in a riverine input close to that of silicate rocks (δ^{98}Mo close to 0.0–0.4 ‰), which differs from the modern riverine flux (0.8 ‰; Archer and Vance, 2008; Revels et al., 2021). Conversely, the transition toward lower weathering intensities - consistent with cold climates associated with strong erosion rates - will tend to shift the riverine Mo isotope flux upwards – in the extreme limit up to the sulfide end-member.

Changes in the riverine Mo isotope flux driven by the factors discussed here may have occurred during the Cenozoic. The sulfur and oxygen isotopes of marine sulfate indicate increasing sulfate fluxes from rivers (driven largely by sulfide oxidation) by a factor of >3, from <1 to $\sim 3 \times 10^{12}$ mol/yr (Waldeck et al., 2022). These interpretations mirror those from other isotope proxy records over the Cenozoic, which also call for changes in sulfide mineral weathering at the global scale (Torres et al., 2014; Caves-Rugenstein et al., 2019). Based on a simple mass balance and assuming a S/Mo ratio of sulfide minerals of $\sim$50–100 $\times 10^3$ mol/mol (Fig. 7), a 3×10^{12} mol/yr change in SO_4 flux from sulfide oxidation would correspond to a $\sim$3–6 $\times 10^7$ mol/yr increase in Mo flux by rivers, equivalent to $\sim$10–20 % of the present-day river Mo flux $\sim 3.1 \times 10^8$ mol/yr (Miller et al., 2011). It remains uncertain how the ratio of sulfide oxidation to silicate mineral weathering changed over the Cenozoic and indeed during other climate and tectonic perturbations of Earth's past. This work suggests that secular changes in seawater Mo isotopes may be expected given the estimated changes in flux and the range in isotope compositions reported here for rivers. However, given the sensitivity of the Mo isotope system to changes in Mo outputs (see Kendall et al., 2017 and the range of variabiliy in sedimentary δ^{98}Mo in Fig. 9), it remains a future research goal to assess whether weathering may be encoded in sedimentary geochemical records.

5. Conclusion

We report the river dissolved and solid isotope compositions of Mo from a set of the world's largest rivers as well as the Mackenzie Basin tributaries. All rivers display significantly higher dissolved δ^{98}Mo compared to the silicate rocks (+0.3 to +1.8 ‰), while river solid δ^{98}Mo ranges from −0.1 to +1.4 ‰.

Dissolved Mo isotope signatures are systematically heavier than their own river suspended particulate matter, reflecting the scavenging of light Mo isotopes into secondary weathering products. In addition, the positive relationship between the riverine dissolved and solid δ^{98}Mo suggests variable weathering from a heavy Mo isotope source. This hypothesis is confirmed by the fact that heavier Mo isotope signatures in the total load exported by rivers are associated with greater Mo export than predicted by silicate rock weathering, a pattern that is difficult to explain in terms of the retention of light Mo isotopes in soils.

River dissolved Mo isotope composition shows broad relationships with silicate vs. sulfide-rich shale tracers. We find that when weathering intensity is high, δ^{98}Mo values of rivers appear to approach the silicate end member. At lower weathering intensities where sedimentary bedrocks are being weathered, the δ^{98}Mo values are higher, and reflect an increased signal from sulfide oxidation. Secular changes in sulfide weathering over geological time could thus impact the δ^{98}Mo of river inputs, impacting our interpretation of past seawater δ^{98}Mo, while potentially providing a way to reconstruct this important weathering flux, which acts as a source of CO_2 to the atmosphere-ocean system.

CRediT authorship contribution statement

Quentin Charbonnier: Writing – review & editing, Writing – original draft, Validation, Methodology, Investigation, Data curation, Conceptualization. **Edward T. Tipper:** Writing – review & editing, Writing – original draft, Resources, Investigation. **Robert G. Hilton:** Writing – review & editing, Writing – original draft, Resources, Investigation. **Corey Archer:** Writing – review & editing, Writing – original draft, Methodology, Formal analysis, Data curation. **Derek Vance:** Writing – review & editing, Writing – original draft, Validation, Supervision, Resources, Investigation, Conceptualization.

Declaration of competing interest

The authors declare that they have no known competing financial interests or personal relationships that could have appeared to influence the work reported in this paper.

Acknowledgements

The authors thank Julien Bouchez and Jérôme Gaillardet for providing some of the samples used in this study. Some of the samples used in this study have been collected in the frame of SEDIMAN project supported by the French Agence Nationale de la Recherche and the Chinese National Science Foundation (grant ANR-15-CE01-0012). This research was supported by Swiss National Science Foundation grant 200021- 184873 to DV. ETT acknowledges NERC funding NE/T007214/1, NE/P011659/1 and NE/M001865/1. Huiming Bao is thanked for her efficient editorial handling of the paper. Three anonymous reviewers are thanked for their constructive comments.

Supplementary materials

Supplementary material associated with this article can be found, in the online version, at doi:10.1016/j.epsl.2025.119368.

Data availability

Data will be made available on request.

References

Archer, C., Vance, D., 2008. The isotopic signature of the global riverine molybdenum flux and anoxia in the ancient oceans. Nat. Geosci 1, 597.
Bouchez, J., Von Blanckenburg, F., Schuessler, J.A, 2013. Modeling novel stable isotope ratios in the weathering zone. Am. J. Sci 313, 267–308.
Bouchez, J., Gaillardet, J., von Blanckenburg, F., 2014. Weathering intensity in lowland river basins: from the Andes to the Amazon mouth. Procedia Earth Planet. Sci 10, 280–286.
Bouchez, J., Gaillardet, J., France-Lanord, C., Maurice, L., Dutra-Maia, P., 2011. Grain size control of river suspended sediment geochemistry: clues from Amazon River depth profiles. Geochem. Geophys, Geosystems 12.
Bufe, A., Hovius, N., Emberson, R., Rugenstein, J.K.C., Galy, A., Hassenruck-Gudipati, H. J., Chang, J.M., 2021. Co-variation of silicate, carbonate and sulfide weathering drives CO2 release with erosion. Nat, Geosci 14, 211–216. https://doi.org/10.1038/s41561-021-00714-3.
Bura-Nakić, E., Andersen, M.B., Archer, C., de Souza, G.F., Marguš, M., Vance, D., 2018. Coupled Mo-U abundances and isotopes in a small marine euxinic basin: constraints on processes in euxinic basins. Geochim. Cosmochim. Acta 222, 212–229.
Calmels, D., Gaillardet, J., Brenot, A., France-Lanord, C., 2007. Sustained sulfide oxidation by physical erosion processes in the Mackenzie River basin: climatic perspectives. Geology 35, 1003–1006.
Charbonnier, Q., Bouchez, J., Gaillardet, J., Calmels, D., Dellinger, M., 2022a. The influence of black shale weathering on riverine barium isotopes. Chem, Geol 594, 120741.
Charbonnier, Q., Bouchez, J., Gaillardet, J., Gayer, E., Porder, S., 2022b. A global imbalance in potassium and barium river export: the result of biological uptake? Geochem. Perspect, Lett 21, 32–36.
Charbonnier, Q., Clarkson, M.O., Hilton, R.G., Vance, D., 2023. Source versus weathering processes as controls on the Mackenzie river uranium isotope signature. Chem, Geol 625, 121409. https://doi.org/10.1016/j.chemgeo.2023.121409.
Charbonnier, Q., Rickli, J., Archer, C., Vance, D., 2024. The influence of secondary weathering processes on dissolved nickel isotope compositions under cold climatic conditions – Observations from the Mackenzie Basin. Geochim. Cosmochim. Acta 364, 10–21.
Clarkson, M.O., Müsing, K., Andersen, M.B., Vance, D., 2020. Examining pelagic carbonate-rich sediments as an archive for authigenic uranium and molybdenum isotopes using reductive cleaning and leaching experiments. Chem, Geol 539, 119412. https://doi.org/10.1016/j.chemgeo.2019.119412.
Dellinger, M., Bouchez, J., Gaillardet, J., Faure, L., Moureau, J., 2017. Tracing weathering regimes using the lithium isotope composition of detrital sediments. Geology 45, 411–414.
Dellinger, M., Gaillardet, J., Bouchez, J., Calmels, D., Galy, V., Hilton, R.G., Louvat, P., France-Lanord, C., 2014. Lithium isotopes in large rivers reveal the cannibalistic nature of modern continental weathering and erosion. Earth Planet, Sci, Lett 401, 359–372.
Dellinger, M., Gaillardet, J., Bouchez, J., Calmels, D., Louvat, P., Dosseto, A., Gorge, C., Alanoca, L., Maurice, L., 2015. Riverine Li isotope fractionation in the Amazon River basin controlled by the weathering regimes. Geochim. Cosmochim. Acta 164, 71–93.
Fang, W., Dai, L.Q., Zheng, Y.F., Zhao, Z.F., 2022. Basalt Mo isotope evidence for crustal recycling in continental subduction zone. Geochim. Cosmochim. Acta 334, 273–292. https://doi.org/10.1016/j.gca.2022.08.008.
Gaillardet, J., Dupré, B., Allègre, C.J., 1999a. Geochemistry of large river suspended sediments: silicate weathering or recycling tracer? Geochim. Cosmochim. Acta 63, 4037–4051.
Gaillardet, J., Dupré, B., Louvat, P., Allègre, C.J., 1999b. Global silicate weathering and CO2 consumption rates deduced from the chemistry of large rivers. Chem, Geol 159, 3–30.
Gaillardet, J., Millot, R., Dupré, B., 2003. Chemical denudation rates of the western Canadian orogenic belt: the Stikine terrane. Chem, Geol 201, 257–279.
Galy, A., France-Lanord, C., 1999. Weathering processes in the Ganges-Brahmaputra basin and the riverine alkalinity budget. Chem, Geol 159, 31–60.
Hartmann, J., Moosdorf, N., 2012. The new global lithological map database GLiM: a representation of rock properties at the Earth surface. Geochem. Geophys, Geosystems 13, 1–37.
Horan, Hilton R.G., Dellinger, M., Tipper, E., Galy, V., Calmels, D., Selby, D., Gaillardet, J., Ottley, C.J., Parsons, D.R., others, Burton K.W., Horan, K., Hilton, R. G., Dellinger, M., Tipper, E., Galy, V., Calmels, D., Selby, D., Gaillardet, J., Ottley, C. J., Parsons, D.R., others, 2019. Carbon dioxide emissions by rock organic carbon oxidation and the net geochemical carbon budget of the Mackenzie River Basin. Am, J. Sci 319, 473–499.
Horan, K., Hilton, R.G., McCoy-West, A.J., Selby, D., Tipper, E.T., Hawley, S., Burton, K. W., 2020. Unravelling the controls on the molybdenum isotope ratios of river waters. Geochem. Perspect, Lett 1–6.
Huh, Y., Birck, J.-L., Allègre, C.J., 2004. Osmium isotope geochemistry in the Mackenzie River Basin. Earth Planet, Sci, Lett 222, 115–129.
Kendall, B., Dahl, T.W., Anbar, A.D., 2017. The stable isotope geochemistry of molybdenum. Rev, Miner., Geochem. 82, 683–732.
King, E.K., Perakis, S.S., Pett-Ridge, J.C., 2018. Molybdenum isotope fractionation during adsorption to organic matter. Geochim. Cosmochim. Acta 222, 584–598. https://doi.org/10.1016/j.gca.2017.11.014.
King, E.K., Pett-Ridge, J.C., 2018. Reassessing the dissolved molybdenum isotopic composition of ocean inputs: the effect of chemical weathering and groundwater. Geology 46, 955–958.
King, E.K., Thompson, A., Chadwick, O.A., Pett-Ridge, J.C., 2016. Molybdenum sources and isotopic composition during early stages of pedogenesis along a basaltic climate transect. Chem, Geol 445, 54–67. https://doi.org/10.1016/j.chemgeo.2016.01.024.
Lemarchand, D., Gaillardet, J., Lewin, A., Allègre, C.J., 2002. Boron isotope systematics in large rivers: implications for the marine boron budget and paleo-pH reconstruction over the Cenozoic. Chem. Geol 190, 123–140.
Levasseur, S., Birck, J.L., Allègre, C.J., 1999. The osmium riverine flux and the oceanic mass balance of osmium. Earth Planet, Sci, Lett 174, 7–23.
Miller, C.A., Peucker-Ehrenbrink, B., Walker, B.D., Marcantonio, F., 2011. *Re*-assessing the surface cycling of molybdenum and rhenium. Geochim. Cosmochim. Acta 75, 7146–7179. https://doi.org/10.1016/j.gca.2011.09.005.
Millot, R., Gaillardet, J., Dupré, B., Allégre, C.J., Allègre, C.J., 2003. Northern latitude chemical weathering rates: clues from the Mackenzie River Basin, Canada. Geochim. Cosmochim. Acta 67, 1305–1329.
Nägler, T.F., Anbar, A.D., Archer, C., Goldberg, T., Gordon, G.W., Greber, N.D., Siebert, C., Sohrin, Y., Vance, D., 2014. Proposal for an international Molybdenum isotope measurement standard and data representation. Geostand, Geoanalytical Res 38, 149–151.
Nägler, T., Pierret, M.C., Voegelin, A., Pettke, T., Aschwanden, L., Villa, I., 2020. Small catchment scale molybdenum isotope balance and its implications for global molybdenum isotope cycling. Biogeochem, Cycles Ecol, Driv. Env., Impact 163–189.
Neely, R.A., Gislason, S.R., Ólafsson, M., McCoy-West, A.J., Pearce, C.R., Burton, K.W., 2018. Molybdenum isotope behaviour in groundwaters and terrestrial hydrothermal systems, Iceland. Earth Planet. Sci. Lett 486, 108–118. https://doi.org/10.1016/j.epsl.2017.11.053.
Négrel, P., Allègre, C.J., Dupré, B., Lewin, E., 1993. Erosion sources determined by inversion of major and trace element ratios and strontium isotopic ratios in river: the Congo Basin case. Earth Planet, Sci, Lett 120, 59–76.
Neubert, N., Heri, A.R., Voegelin, A.R., Nägler, T.F., Schlunegger, F., Villa, I.M., 2011. The molybdenum isotopic composition in river water: constraints from small catchments. Earth Planet, Sci, Lett 304, 180–190. https://doi.org/10.1016/j.epsl.2011.02.001.
O'Sullivan, E.M., Nägler, T.F., Babechuk, M.G., 2021. Unusually heavy stable Mo isotope signatures of the Ottawa River: causes and implications for global riverine Mo fluxes. Chem, Geol 568.
Pearce, C.R., Burton, K.W., von Strandmann, P.A.E.P., James, R.H., Gíslason, S.R., 2010. Molybdenum isotope behaviour accompanying weathering and riverine transport in a basaltic terrain. Earth Planet, Sci, Lett 295, 104–114. https://doi.org/10.1016/j.epsl.2010.03.032.
Peucker-Ehrenbrink, B., Jahn, 2001. the Upper Continental Crust. Geochem. Geophys, Geosystems 2, 1–22.
Rahaman, W., Goswami, V., Singh, S.K., Rai, V.K., 2014. Molybdenum isotopes in two Indian estuaries: mixing characteristics and input to oceans. Geochim. Cosmochim. Acta 141, 407–422. https://doi.org/10.1016/j.gca.2014.06.027.
Relph, K.E., Stevenson, E.I., Turchyn, A.V., Antler, G., Bickle, M.J., Baronas, J.J., Darby, S.E., Parsons, D.R., Tipper, E.T., 2021. Partitioning riverine sulfate sources using oxygen and sulfur isotopes: implications for carbon budgets of large rivers. Earth Planet, Sci, Lett 567, 116957. https://doi.org/10.1016/j.epsl.2021.116957.
Revels, B.N., Rickli, J., Moura, C.A.V., Vance, D., 2021. The riverine flux of molybdenum and its isotopes to the ocean: weathering processes and dissolved-particulate partitioning in the Amazon basin. Earth Planet, Sci, Lett 559, 116773. https://doi.org/10.1016/j.epsl.2021.116773.
Ross, D.J.K., Bustin, R.M., 2009. Investigating the use of sedimentary geochemical proxies for paleoenvironment interpretation of thermally mature organic-rich strata: examples from the devonian-mississippian shales. West. Can. Sediment. Basin, Chem, Geol 260, 1–19. https://doi.org/10.1016/j.chemgeo.2008.10.027.

Rudnick, R.L., Gao, S., 2013. Compos. Cont. Crust 1–51. *Treatise on Geochemistry: Second Edition*.
Rugenstein, J.K.C., Ibarra, D.E., von Blanckenburg, F., 2019. Neogene cooling driven by land surface reactivity rather than increased weathering fluxes. Nature 571, 99.
Sharma, M., Wasserburg, G.J., Hofmann, A.W., Chakrapani, G.J., 1999. Himalayan uplift and osmium isotopes in oceans and rivers - its relation to global tectonics and climate. Geochim. Cosmochim. Acta 63, 4005–4012. https://doi.org/10.1016/S0016-7037(99)00305-1.
Spence, J., Telmer, K., 2005. The role of sulfur in chemical weathering and atmospheric CO2 fluxes: evidence from major ions, δ13CDIC, and δ34SSO4 in rivers of the Canadian Cordillera. Geochim. Cosmochim. Acta 69, 5441–5458.
Stallard R.F. and Edmond J.M. (1981) of Geological and GeophysiCal. *October* 86, 9844–9858.
Taylor, S.R., McLennan, S.M., 1995. The geochemical evolution of the continental crust. Rev, Geophys 33, 241–265.
Tipper, E.T., Calmels, D., Gaillardet, J., Louvat, P., Capmas, F., Dubacq, B., 2012. Positive correlation between Li and Mg isotope ratios in the river waters of the Mackenzie Basin challenges the interpretation of apparent isotopic fractionation during weathering. Earth Planet, Sci, Lett 333, 35–45.
Tipper, E.T., Stevenson, E.I., Alcock, V., Knight, A.C.G., Baronas, J.J., Hilton, R.G., Bickle, M.J., Larkin, C.S., Feng, L., Relph, K.E., Hughes, G., 2020. Global silicate weathering flux overestimated because of sediment-water cation exchange. Proc, Natl, Acad, Sci, U. S. A 118.
Torres, M.A., Moosdorf, N., Hartmann, J., Adkins, J.F., West, A.J., 2017. Glacial weathering, sulfide oxidation, and global carbon cycle feedbacks. Proc. Natl. Acad. Sci 114, 8716–8721.
Torres, M.A., West, A.J., Clark, K.E., Paris, G., Bouchez, J., Ponton, C., Feakins, S.J., Galy, V., Adkins, J.F., 2016. The acid and alkalinity budgets of weathering in the Andes–Amazon system: insights into the erosional control of global biogeochemical cycles. Earth Planet. Sci. Lett 450, 381–391.
Torres, M.A., West, A.J., Li, G., 2014. Sulphide oxidation and carbonate dissolution as a source of CO2 over geological timescales. Nature 507, 346.
Voegelin, A.R., Nägler, T.F., Pettke, T., Neubert, N., Steinmann, M., Pourret, O., Villa, I. M., 2012. The impact of igneous bedrock weathering on the Mo isotopic composition of stream waters: natural samples and laboratory experiments. Geochim. Cosmochim. Acta 86, 150–165.
Waldeck, A.R., Hemingway, J.D., Yao, W., Paytan, A., Johnston, D.T., 2022. The triple oxygen isotope composition of marine sulfate and 130 million years of microbial control. Proc, Natl, Acad, Sci, U. S. A 119.
Walsh, E.V., Hilton, R.G., Tank, S.E., Amos, E., 2024. Temperature sensitivity of the mineral permafrost feedback at the continental scale. Sci, Adv 10, eadq4893.
Wang, Z., Ma, J., Li, J., Wei, G., Chen, X., Deng, W., Xie, L., Lu, W., Zou, L., 2015. Chemical weathering controls on variations in the molybdenum isotopic composition of river water: evidence from large rivers in China. Chem, Geol 410, 201–212. https://doi.org/10.1016/j.chemgeo.2015.06.022.
Wang, Z., Ma, J., Li, J., Wei, G., Zeng, T., Li, L., Zhang, L., Deng, W., Xie, L., Liu, Z., 2018. Fe (hydro) oxide controls Mo isotope fractionation during the weathering of granite. Geochim. Cosmochim. Acta 226, 1–17. https://doi.org/10.1016/j.gca.2018.01.032.
West, A.J., Galy, A., Bickle, M., 2005. Tectonic and climatic controls on silicate weathering. Earth Planet, Sci, Lett 235, 211–228.
Willbold, M., Elliott, T., 2017. Molybdenum isotope variations in magmatic rocks. Chem, Geol 449, 253–268.
Ye, Y., Zhang, S., Wang, H., Wang, X., Tan, C., Li, M., Wu, C., Canfield, D.E., 2021. Black shale Mo isotope record reveals dynamic ocean redox during the mesoproterozoic era. Geochem. Perspect, Lett 18, 16–21.